# CHARACTERIZATION, MECHINICAL, THERMAL AND ABLATIVE PROPERTIES OF CERAMIC MODIFIED PHENOLIC RESIN AEROGELS SYNTHSIZED BY AMBIENT PRESSURE DRYING

Jun Zhang[1, 2], Rongying Yin[3], Haiming Cheng[1,*], Changqing Hong[1], Xinghong Zhang[1] and Songhe Meng[1]

[1] National Key Laboratory of Science and Technology on Advanced Composites in Special Environments, Harbin Institute of Technology, Harbin, 150080, P. R. China
[2] China Aerodynamics Research and Development Center, Mianyang, 621000, P. R. China
[3] Harbin Aircraft industry (Group) Co. Ltd, Aviation Industry Corporation of China, Harbin, 150060, P. R. China
***Corresponding author:** Haiming Cheng (hmingcheng@163.com)

**Keywords:** Ceramic, Phenolic resin, Aerogel, Mechanical Properties, Thermal Properties

## ABSTRACT

During the past few decades, various organic aerogels (AGs) have been synthesized and shown a number of exceptional and even unique properties, such as low bulk density, high porosity, great surface areas, and extremely low thermal conductivity, which enable them being the focus of industry and academia. Thus, AGs exhibit substantial performance boosts in numerous applications such as adsorption, separation, catalysis, energy conversion and storage, and so on. Regrettably, AGs generally exhibit high cost, poor thermal and mechanical properties, which seriously restrict their large-scale applications. In this study, ceramic was introduced into commercial available resin derived aerogel due to the enhancement of silicon to thermal stability and low cost of the resin. Silica ceramic modified phenolic resin (PR-$SiO_2$) aerogel was synthesized by a simple sol-gel polymerization of ceramic precursor, PR, hexamethylenetetramine in an ethylene glycol solution, followed by solvent exchange and ambient pressure drying. The modified effect on the porous structure, textural property, and thermal stability was studied by scanning electron microscope (SEM), nitrogen adsorption isotherms, and thermogravimetric analysis (TGA). According to the characterizations of SEM and nitrogen adsorption, the obtained PR-$SiO_2$ hybrid aerogels have a continuous three dimensional network that consists of phenolic nano-particles and curved nano-sheets with size from 50 to 90 nm, which define numerous mesopores and macropores. TGA in argon atmosphere indicated that the thermal stability of the PR-$SiO_2$ aerogels (both maximum decomposition rate and char yield at 1000 ℃) is better than that of the pristine PR aerogel. In order to improve the mechanical properties, carbon fabric reinforced aerogel composite was prepared by impregnating carbon-bonded carbon fiber (CBCF) composite with the aerogels. In the micrographs of the aerogel matrix composite, the aerogels are fully and uniformly occupied the void between carbon fibers, and coated with a thin layer on the fiber surface. Moreover, a homogeneous morphology without cracking and fracture was obtained at the fiber/resin interface, as the appropriate porous structure and enough strength of the aerogel networks to decrease and withstand the capillary pressure at the liquid/gas interface during the drying at ambient pressure, prevent the aerogel networks from collapse. Due to the low bulk density (0.18g/$cm^3$), high porosity (~90%) and unique fiber geometry (a typical 2D planar random structure with the carbon fibres in the xy direction are distributed homogeneously in plane, while in the z direction over the height of the composite) of the CBCF fabric, the obtained composite possessed low bulk density (0.32-0.45 g/$cm^3$), high compressive strength (0.8-2.8 MPa for different directions) and low thermal conductivity (0.098-0.148 W/(mK)). More importantly, good thermal ablative and insulative properties in oxy-acetylene flame simulated high temperature environment (linear ablation rate as low as 0.085 mm/s, internal temperature peaks below 200 ℃ at 38 mm in-depth position as the surface temperature approximately 1800 ℃). Therefore, the novel lightweight aerogels and composites are excellent heat-insulation and thermal-protection materials with applications in the fields of energy-saving and aerospace.

## 1 INTRODUCTION

Aerogels, three-dimensional solids of colloidal particles, have enormous applications including adsorption, separation, catalysis, energy conversion and storage [1, 2], originated from the advantages of low density, high pore volumes, large surface areas, and extremely low thermal conductivity. Furthermore, they have potential for high temperature thermal protection and insulation applications in aerospace industry [3, 4]. However, the wide applications have been hindered seriously due to the high cost of raw materials, the long time consuming of sol-gel method as well as the personal safety risks and the complexity of processing of supercritical drying, together with the poor mechanical behaviour derived from the inherent microstructure of aerogels [5, 6].

In order to overcome the above mentioned limitations, ambient pressure drying (APD) synthesis of aerogels used cheap commercial available resin prepolymers as precursor, such as phenolic resin (PR), polyvinyl alcohol, epoxy, and polyimide [7-10], has drawn considerable research attention and should be a practicable countermeasure for solving these problems. T. Lu's group [11, 12], Y. Zhang et al. [13, 14], X. Jia et al. [15], etc., made an excellent research on fabrication carbon aerogels through the sol-gel polymerization of PR prepolymer. Moreover, various approaches have been explored to improve the mechanical and thermal properties cross-linking silica or graphene into aerogel backbone resulting in hybrid aerogels by co-precursor method [16, 17].

Furthermore, improving mechanical properties of aerogels is the foundation for many potential applications. Extensive efforts have been made on mechanically reinforcing aerogels via developing aerogel composites. In various attempts, reinforcing aerogels with low-density fabrics, with the help of the structural support, the resulting aerogel composites demonstrate superior properties due to synergistic interactions [18].

In this study, a simple sol-gel polymerization of PR, methyltrimethoxysilane (MTMS) and hexamethylenetetramine (HMTA) in an ethylene glycol (EG) solution, followed by solvent exchange and APD, was design to prepare low density and thermal stable strong phenolic resin/silica (PR-$SiO_2$) hybrid aerogels. Furthermore, a lightweight carbon-bonded carbon fiber (CBCF) composite as reinforcement was employed to prepare aerogel matrix composite, the high porosity and unique fibre geometry of the carbon fabric also result in low density, low thermal conductivity and relatively high mechanical properties in the obtained composite. Ablation performance of the composite was evaluated in the severe hyperthermal environment simulated by an oxy-acetylene flame system.

## 2 EXPERIMENTAL

### 2.1 MATERIALS

HMTA, MTMS, EG and anhydrous ethanol (EtOH) were purchased from Aladdin Industrial Inc. All chemicals were analytical grade and used as received. PR solution has concentration of 66.7 wt% with EtOH was purchased from Shaanxi Taihang Impede-fire Polymer Co. Ltd., China. CBCF composite with a density of 0.184 g/$cm^3$ was prepared according to the literature [19].

### 2.2 SYNTHESIS OF CBCF/PR-SILICA AEROGEL COMPOSITE

In the typical process, 0.04 mol (5.449g) of MTMS, 20.000 g PR and 2.000 g HMTA were added and dissolved sequentially in 80.000 g EG which stirred mechanically at room temperature. The resulting mixture was mechanical stirred for 30 min to obtain a homogeneous solution, and then the CBCF composite (with density of 0.18 g/$cm^3$) was immersed and impregnated into the solution. This process was assisted by vacuum piping to ensure the solution fully infiltrated in the fabric. Then the systems were heated using the procedure of heating at 90 ℃ for 1 h, at 120 ℃ for 3 h, and finally at 180 ℃ for 3 h. Next, the wet-gel impregnated CBCF composite was immersed in EtOH to remove EG from the pores at 60 ℃ for 3 days. Finally, the composite was dried in air under ambient pressure at room temperature (≤30 ℃) until constant weight was obtained. This resulted in CBCF/PR-$SiO_2$ aerogel composites with densities of 0.34 g/$cm^3$. Additionally, pristine CBCF/PR composite (with density of 0.31 g/$cm^3$) as the control sample was fabricated with a precursor solution only containing PR, HMTA and EG in the same way.

### 2.3 CHARACTERIZATION

Microstructure was observed on an FEI Quanta 200FEG field emission scanning electron microscope (FE-SEM). $N_2$ adsorption and desorption isotherms were recorded by a Micromeritics ASAP 2020 V3.00 H adsorption apparatus. The thermal stability was analyzed by NETZSCH TG 209C thermogravimetric analyzer (TGA) at a rate of 10 ℃/min under an argon atmosphere. The Fourier transformed infrared (FTIR) spectra were recorded between 500 and 4000 $cm^{-1}$ from KBr pellets by Bruker Tensor 27 Spectrophotometer. Compression testing was carried out on an Instron 5569 universal test machine with the loading rate of 0.5 mm/min using at least five specimens with dimensions of 10 × 10 × 12 $mm^3$ for each sample. Thermal conductivity in z direction at room temperature was measured on a Hot Disk TPS 2500 thermal constant analyzer, based on the transient hot plane method, using square-shaped specimen with dimensions of 30 × 30 × 20 $mm^3$.

Ablative properties of the CBCF/PR-$SiO_2$ aerogel composite were evaluated in the severe hyperthermal environment simulated by using an oxy-acetylene flame system. During the test, distance between nozzle tip of the oxyacetylene gun and sample was kept constant at 40 mm, and inner diameter of the tip was 2.0 mm. Flow rates of oxygen ($O_2$) and acetylene ($C_2H_2$) were maintained at 0.4 and 0.5 $m^3$/h, respectively, and the flame flux was estimated to be approximately 1.1 $MW/m^2$ measured using a copper slug calorimeter. Surface and internal temperature of the sample was monitored by an infrared pyrometer and K-type thermocouples. Three thermocouples were fitted at 20, 30 and 38 mm in-depth from the front surface in the sample, and the external body of thermocouples was protected using double barreled alumina tubes. The sample, fixed in a shield holder consist of graphite holder and heat insulation ring made of chopped glass fiber reinforced phenolic resin composite, was exposed to the flame for 120 s. At least three samples with *iso-q* shape were examined in each test, the sample was a cylinder with a spherical nose, the nose radius and cylinder diameter are both 20.0 mm, the shoulder radius is 1.25 mm, the length is 40 mm [20]. Also, the changes in shape during the testing process were also received and recorded by CCD image sensor. The ablation test was carried out to evaluate linear ablative rate and mass ablative rate, and they were calculated using the following formulas:

$$\text{Linear ablation rate } (A_{RL}) = (L_o - L_a)/t \quad (1)$$

$$\text{Mass ablation rate } (A_{RM}) = (M_o - M_a)/t \quad (2)$$

where $A_{RL}$ is linear ablation rate (mm/s), $A_{RM}$ is mass ablation rate (g/s), $L_o$ and $L_a$ are thickness (mm) of samples before and after ablation test, $M_o$ and $M_a$ are mass (g) of sample measured before and after ablation test and $t$ is ablation time (s) [21].

## 3 RESULTS AND DISCUSSION

### 3.1 MICROSTRUCTURE AND TEXTURAL PROPERTIES OF CBCF/PR AND CBCF/PR-$SIO_2$ AEROGEL COMPOSITE

The microstructure of CBCF and the CBCF/PR-$SiO_2$ aerogel composites in the xy plane and z direction are shown in Fig. 1. Micrographs of the as-prepared CBCF (Fig. 1a and b) show the classic anisotropic structure of the CBCF composite, the chopped carbon fibres in the xy direction are distributed with randomly and uniformly in plane, and uniformly distributed over the height of the composite in the z direction. The carbon fibres are linked together at the crossing points of adjacent fibres with pyrolytic carbon to form a three-dimensional structure and the width of the fiber-lap holes is larger than tens of microns. After the impregnation of PR-$SiO_2$ aerogels, the fibrous framework is homogeneously filled by aerogels and the surface of fiber is covered by aerogels, as shown in Fig. 1c and d. It can be found that a superior fiber/resin interface without cracking or deboning was achieved (as insert in Fig. 1c), which may result the appropriate pore structure (as insert Fig. 1d) and enough strength of the aerogel networks to decrease and withstand the capillary pressure during the APD, prevent the aerogel networks from collapse.

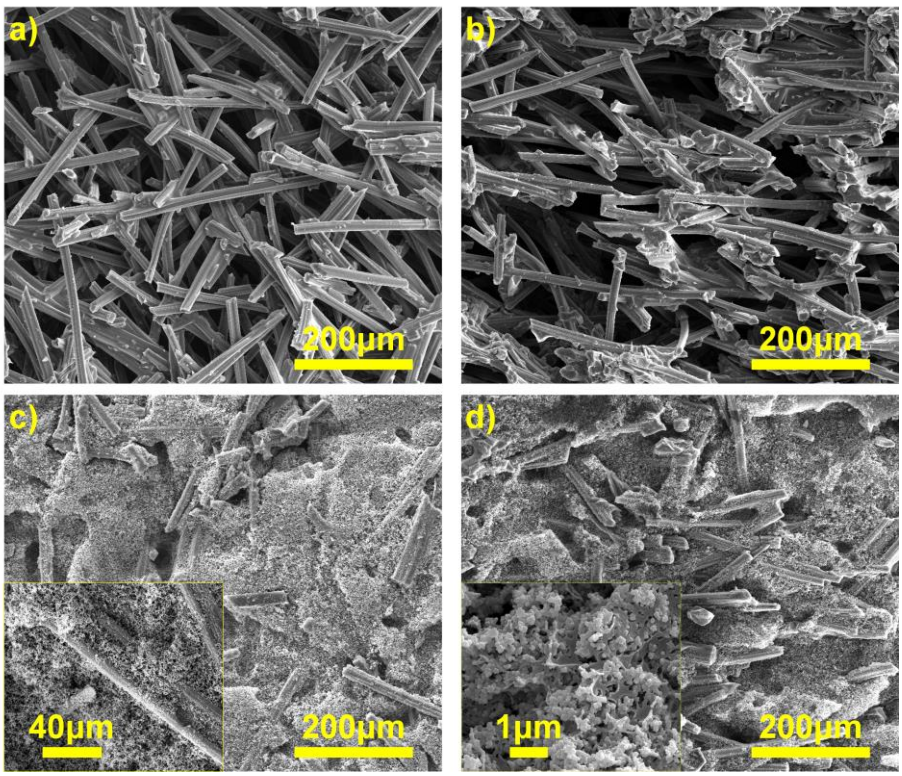


Figure 1 a and b) Microstructure of the CBCF and c and d) the CBCF/PR-Si aerogel composite in the xy and z direction, respectively. Insert: High magnification images of the aerogel composite and PR-$SiO_2$ hybrid aerogels.

To examine the pore structure PR-$SiO_2$ aerogels, $N_2$ sorption measurement was performed. Fig. 2a and b exhibit the $N_2$ adsorption-desorption isotherms of PR and PR-$SiO_2$ aerogels after APD. All of them exhibit typical Type IV isotherms and H3 hysteresis loops at high relative pressure according to the IUPAC classification, indicating the presence of meso- and macropores [22]. It can be seen that the sorption capacity increases after the addition of MTMS, this could be contributed to a denser network structure was formed (insert in Fig.1d) as aerogel density increased after the modification, thus macropores that may not be detected by $N_2$ sorption was occupied by aerogel particles and more micro- and mesopores were formed simultaneously. The surface area, pore volume and pore size distribution of samples were calculated from their desorption isotherms by BJH method, and the results are summarized in Table 1. The pore size distributions (insert in Fig. 2a and b) of PR and PR-$SiO_2$ both display broad peak of combination of meso- and macropores centred at 30-60 nm. Moreover, both the calculated surface area and pore volume increase (Table 1), indicating the important effect of ceramic modification on porosity developments in the aerogels.

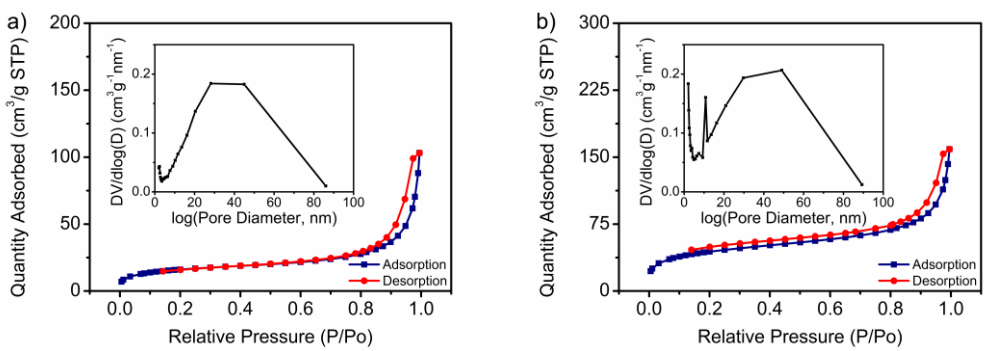

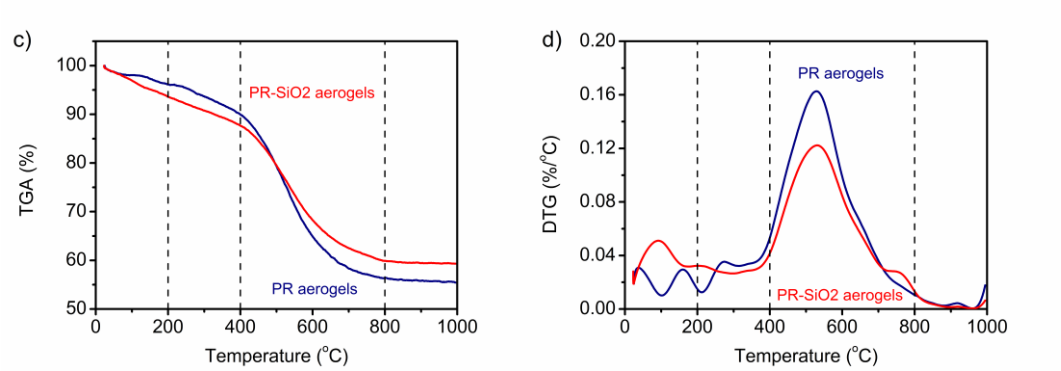


Fig. 2 a) $N_2$ adsorption and desorption isotherms and b) BJH pore size distribution curves at 77 K, STP = standard temperature and pressure; $P/P_o$ = the ratio of the adsorption pressure (P) and the saturation vapor pressure ($P_o$); c) TGA and d) DTG curves of PR aerogels and PR-$SiO_2$ composite aerogel, respectively.

| Sample | $S_{BET}$ ($m^2/g$) | $S_{Micro}$ ($m^2/g$) | $S_{Meso}$ ($m^2/g$) | $V_{Micro}$ ($cm^3/g$) | $V_{Meso}$ ($cm^3/g$) | $T_{5\%}$ (℃) | $T_{10\%}$ (℃) | $T_{d,max}$ (℃) | $R_{1000\ ℃}$ (%) |
|---|---|---|---|---|---|---|---|---|---|
| PR | 58.422 | 9.315 | 41.234 | 0.003 | 0.155 | 262.40 | 399.29 | 526.10 | 55.44 |
| PR-$SiO_2$ | 158.146 | 36.781 | 94.207 | 0.015 | 0.213 | 155.15 | 327.80 | 533.16 | 59.32 |

Table 1 Textrual and thermal characteristics of the PR and PR-$SiO_2$ hybrid aerogels.
Note: $S_{BET}$: BET surface area; $S_{Micro}$: micropore surface area; $S_{Meso}$: BJH Desorption cumulative surface area of pores Between 1.7 and 300 nm diameter; $V_{Micro}$: micropore volume; $V_{Meso}$: BJH desorption cumulative pore volume of pores between 1.7 and 300 nm diameter. $T_{5\%}$: Thermal decomposition temperature at 5% weight loss; $T_{10\%}$: Thermal decomposition temperature at 10% weight loss; $T_{d,max}$: Maximum rate of the weight loss; $R_{1000\ ℃}$: Residual weight at 1000 ℃.

Thermal stability and degradation behaviour of PR and PR-$SiO_2$ aerogels was investigated by TGA from room temperature to 1000 ℃ under an argon atmosphere. The results are depicted in Fig. 2c and d. It is easy to notice the improvement of introducing MTMS on the thermal stability, from the TGA curves PR-$SiO_2$ aerogels possessed higher residual weight than the PR aerogels after pyrolysis temperature exceeding 400 ℃. Moreover, in the DTG curves, the maximum decomposition rate ($D_{Max}$, the peak at temperature around 530 ℃) of the PR-$SiO_2$ aerogels is much lower than that of PR aerogels. Besides, the residual weight at 1000 ℃ ($R_{1000\ ℃}$) exhibits the same trend, indicating the enhancement of thermal stability.

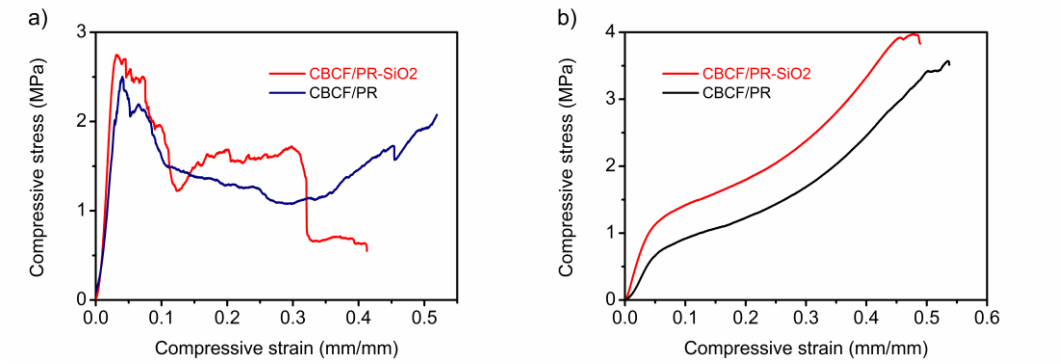


Fig. 3 Representative compressive stress vs. strain curves of CBCF/PR and CBCF/PR-$SiO_2$ aerogels composite in the xy and z directions, respectively.

Compression tests were carried out on CBCF/PR and CBCF/PR-$SiO_2$ aerogels composite to investigate the mechanical behaviour of the aerogel composite. Fig. 3a and b show the representative compressive stress vs. strain curves in the xy and z direction under ambient conditions. The compressive response of the composites were similar to those of CBCF with low densities or pyrolytic carbon (and/or ceramic) coated CBCF, demonstrating a linear elastic region up to approximately 4-5% strain and yield up to approximately 50-70% strain. The elastic deformation was believed to be formed through elastic bending and rotation of fibers, the denser and stronger ceramic modified aerogels filled in the voids between carbon fibres and coated on the fibre surface could restrict the fiber locomotion more effectively, so mechanical properties (both compressive strength and Yong's modulus) were enhanced after the addition of MTMS.

Thermal conductivity for CBCF/PR and CBCF/PR-SiO2 aerogels composite samples were measured at room temperature, and the results were depicted in table 2, the aerogels composites exhibit rather low thermal conductivity of 0.098 and 0.148 W/(mK), which made this material a potential candidate as the high-temperature thermal insulator. The low thermal conductivity was mainly attributed to fibre/aerogel composite structure in the material that the three dimensional nanostructure wraps the fibre skeleton, impairing the heat transfer across the aerogel matrix.

### 3.2 ABLATION PERFORMANCE OF CBCF/PR-$SIO_2$ AEROGEL COMPOSITE

The thermal ablative property of the CBCF/PR-$SiO_2$ aerogel composite was evaluated under high temperature environment simulated by an oxyacetylene torch test apparatus, and the linear and mass ablation rate was calculated, and the results was shown in Table 2. Fig. 4 show the images of the aerogel composite before, during and after the ablation test. The better ablation resistance of the CBCF/PR-$SiO_2$ aerogel composite compared to the original CBCF/PR composite can be observed from the significant reduction in the change in shape of sample and ablation rate. It is easy to understand that the higher char yield of the PR-$SiO_2$ aerogels means more resin decomposition product and pyrolytic carbon remains, therefore more effectively insulate the materials beneath the ablation surface.

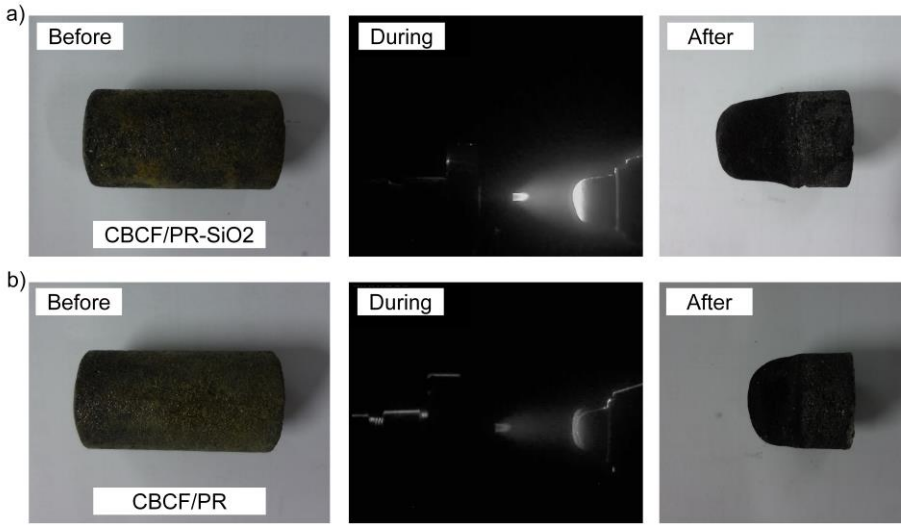


Fig. 4 Sample CBCF/PR-$SiO_2$ and CBCF/PR before and after oxy-acetylene flame ablation test.

Surface and internal temperature histories during plasma exposure and cooldown period afterwards were depicted in Fig. 5. The surface temperature was found to quickly reach over 2000 ℃ after sample exposure, and kept at a relatively high value during the test. It is favored for the char ablation materials, thus a great mass of the heat can be reradiation continually to the boundary layer avoiding a high heat transfer into the internal structure by heat conduction [23]. While the surface temperature is exceeding 2000 ℃, the internal temperature peaks at about only 580 ℃ at 30 mm in-depth from the

surface (Fig. 5 and Table 2). Even more dramatic is that, at 38 mm the peaks were no more than 200 ℃. This demonstrates the fairly good insulative properties of CBCF/PR and CBCF/PR-$SiO_2$ aerogel composite. Also indicates that most of the heat was rejected by a reradiation mechanism, for the high porosity of the composite (Fig. 1), the heat is being rejected at the surface rather than stored in heat conduction.

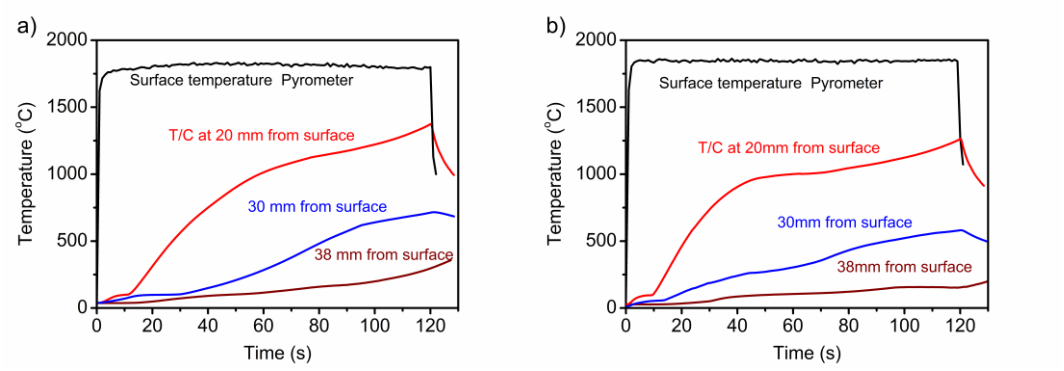


Fig. 5 a and b) Surface and internal temperature responses of CBCF/PR and CBCF/PR-$SiO_2$ measured by infrared pyrometer from initial stagnation point and thermocouples located at 20, 30 and 38 mm in-depth during the high temperature flame exposure, respectively.

| Sample | Thermal conductivity (W/(mK)) | $A_{RL}$ (mm/s) | $A_{RM}$ (g/s) | Temperature peak (℃) | | | |
|---|---|---|---|---|---|---|---|
| | | | | Surface | T/C at 20cm | T/C at 30cm | T/C at 38cm |
| CBCF/PR | 0.098 | 0.085 | 0.020 | 1833 | 1374.3 | 712.4 | 296.4 |
| CBCF/PR-$SiO_2$ | 0.148 | 0.119 | 0.018 | 1863 | 1263.4 | 581.3 | 154.2 |

Table 2 Ablation testing results of CBCF/PR and CBCF/PR-$SiO_2$ aerogel composite.
*Note:* $A_{RL}$ and $A_{RM}$: linear and mass ablation rate; $L_o$ and $L_a$: thickness (mm) of samples before and after ablation test, $M_o$ and $M_a$: mass of sample measured before and after ablation test; $t$: ablation time.

## 9 CONCLUSIONS

In summary, a simple sol-gel polymerization process was developed to fabricate lightweight PR-$SiO_2$ hybrid aerogels and CBCF/PR-$SiO_2$ aerogel composite exhibiting high thermal stability, good mechanical properties and low thermal conductivity. More importantly, good thermal ablative and insulative properties (linear ablation rate as low as 0.085 mm/s, internal temperature peaks below 200 ℃ at 38 mm in-depth position when the surface temperature approximately 1800 ℃) under high temperature oxyacetylene flame. Thus, the novel aerogels and composites are capable of lightweight thermal protection and insulation applications.

## ACKNOWLEDGEMENTS

This work is financially supported by the National Natural Science Foundation of China (grant Nos. 11572353, 51272056, 11121061 and 91216301); the foundation for Innovative Research Groups of the National Natural Science Foundation of China (grant No. 11421091); and the National Science Fund for Distinguished Young Scholars of China (grant No. 51525201).

## REFERENCES

[1] Y. Fang, Y. Lv, F. Gong, A.A. Elzatahry, G. Zheng and D. Zhao, Synthesis of 2D-mesoporou-carbon/MoS2 heterostructures with well-defined interfaces for high-performance lithium-ion batteries, *Advanced Materials,* **28**, 2016, pp. 9385-9390 (doi: 10.1002/adma.201602210).

[2] S.L. Candelaria, R. Chen, Y.H. Jeongd and G. Cao, Highly porous chemically modified carbon cryogels and their coherent nanocomposites for energy applications, *Energy & Environmental Science*, **5,** 2012, pp. 5619-5637 (doi: 10.1039/C1EE02634H).
[3] J.P. Randall, M.A.B. Meador and S.C. Jana, Tailoring mechanical properties of aerogels for aerospace applications, *ACS Applied Materials & Interfaces*, **3**, 2011, pp.613-626 (doi: 10.1021/am200007n).
[4] J. Feng, C. Zhang, J. Feng, Y. Jiang and N. Zhao, Carbon aerogel composites prepared by ambient drying and using oxidized polyacrylonitrile fibers as reinforcements, *ACS Applied Materials & Interfaces*, **3,** 2011, pp. 4796-4803 (doi: 10.1021/am201287a).
[5] N. Leventis, N. Chandrasekaran, A.G. Sadekar, C. Sotiriou-Leventis and H. Lu, One-pot synthesis of interpenetrating inorganic/organic networks of CuO/resorcinol-formaldehyde aerogels: nanostructured energetic materials, *Journal of the American Chemical Society*, **131**, 2009, pp. 4576-4577 (doi: 10.1021/ja809746t).
[6] M. Schwan, R. Tannert and L. Ratke, New soft and spongy resorcinol–formaldehyde aerogels, *The Journal of Supercritical Fluids*, **107**, 2016, pp. 201-208 (doi: 10.1016/j.supflu.2015.09.010).
[7] C. Chidambareswarapattar, Z. Larimore, C. Sotiriou-Leventis, J.T. Mang and N. Leventis, One-step room-temperature synthesis of fibrous polyimide aerogels from anhydrides and isocyanates and conversion to isomorphic carbons, *Journal of Materials Chemistry*, **20**, 2010, pp. 9666-9678 (doi: 10.1039/C0JM01844A).
[8] S. Ye, J. Feng and P. Wu, Highly elastic graphene oxide-epoxy composite aerogels via simple freeze-drying and subsequent routine curing, *Journal of Materials Chemistry A*, **1**, 2013, pp. 3495-3502 (doi: 10.1039/C2TA01142E ).
[9] J. Guo, B.N. Nguyen, L. Li, M.A.B. Meador, D.A. Scheimanb and M. Cakmak, Clay reinforced polyimide/silica hybrid aerogel, *Journal of Materials Chemistry A*, **1**, 2013, pp. 7211-7221 (doi: 10.1039/C3TA00439B).
[10] A. Szczurek, K. Jurewicb, G. Amaral-Labat, V. Fierro, A. Pizzi and A. Celzard, Structure and electrochemical capacitance of carbon cryogels derived from phenol–formaldehyde resins, *Carbon*, **48**,2010, pp.3874-3883 (doi: 10.1016/j.carbon.2010.06.053).
[11] S. Xu, J. Li, G. Qiao, H. Wang and T. Lu, Pore structure control of mesoporous carbon monoliths derived from mixtures of phenolic resin and ethylene glycol, *Carbon*, **47**, 2009, pp. 2103-2111 (doi: 10.1016/j.carbon.2009.03.069).
[12] S. Xu, G. Qiao, H. Wang, D. Li and T. Lu, Preparation of mesoporous carbon derived from mixtures of phenol-formaldehyde resin and ethylene glycol, *Materials Letters*, **62**, 2008, pp. 3716-3718 (doi: 10.1016/j.matlet.2008.04.037).
[13] Y. Zhang, Z. Yuan and Y. Zhou, Effect of furfural alcohol/phenol-formaldehyde resin mass ratio on the properties of porous carbon, *Materials Letters*, **109**, 2013, pp. 124-126 (doi: 10.1016/j.matlet.2013.07.053).
[14] Y. Zhang, Z. Yuan, Y. Zhou and J. Han, Preparation and characterization of porous carbons obtained from mixtures of furfuryl alcohol and phenol–formaldehyde resin, *Materials Chemistry and Physics*, **143**, 2014, pp. 707-712 (doi: 10.1016/j.matchemphys.2013.10.001).
[15] X. Jia, B. Dai, Z. Zhu, J. Wang, W. Qiao, D. Long and L. Ling, Strong and machinable carbon aerogel monoliths with low thermal conductivity prepared via ambient pressure drying, *Carbon*, **108**, 2016, pp. 551-560 (doi: 10.1016/j.carbon.2016.07.060).
[16] K. Guo, Z. J. Hu, H. H. Song, X. Du, L. Zhong and X. H. Chen, Low-density graphene/carbon composite aerogels prepared at ambient pressure with high mechanical strength and low thermal conductivity, *RSC Advances*, **5**, 2015, pp. 5197-5204 (doi: 10.1039/C4RA08800J).
[17] S. Yun, H. Luo and Y. Gao, Ambient-pressure drying synthesis of large resorcinol–formaldehyde-reinforced silica aerogels with enhanced mechanical strength and superhydrophobicity, *Journal of Materials Chemistry A*, **2**, 2014, pp. 14542-14549 (doi: 10.1039/C4TA02195A).
[18] M. Antonietti, N. Fechler and T.P. Fellinger, Carbon aerogels and monoliths: control of porosity and nanoarchitecture via sol-gel routes, *Chemistry of Materials*, **26**, 2013, pp. 196-210 (doi: 10.1021/cm402239e).

[19] C. Liu, J. Han, X. Zhang, C. Hong and S. Du, Lightweight carbon-bonded carbon fiber composites prepared by pressure filtration technique, *Carbon*, **59**, 2013, pp. 547–554 (doi: 10.1016/j.carbon.2013.03.049).
[20] H. Weng, S.C.C. Bailey and A. Martin, Numerical study of iso-Q sample geometric effects on charring ablative materials, *International Journal of Heat and Mass Transfer*, **80**, 2015, pp. 570–596 (doi: 10.1016/j.ijheatmasstransfer.2014.09.040).
[21] C. Sun, H. Li, Q. Fu and J. Zhang, Microstructure and ablation properties of carbon/carbon composites modified by ZrSiO4, *Corrosion Science*, **79**, 2014, pp. 100-107 (doi: 10.1016/j.corsci.2013.10.031)
[22] M. Kruk and M. Jaroniec, Gas adsorption characterization of ordered organic-inorganic nanocomposite materials, *Chemistry of Materials*, **13**, 2001, pp. 3169-3183 (doi: 10.1021/cm0101069).
[23] A. Mazzaracchio and M. Marchetti, A probabilistic sizing tool and Monte Carlo analysis for entry vehicle ablative thermal protection systems, *Acta Astronautica*, **66**, 2010, pp. 821-835 (doi: 10.1016/j.actaastro.2009.08.033).